Polarization-resolved second harmonic generation microscopy with a four-channel Stokes-polarimeter

Nirmal Mazumder,[1] Jianjun Qiu,[1] Matthew R. Foreman,[2] Carlos Macías Romero,[2] Chih-Wei Hu,[1] Han-Ruei Tsai,[1] Peter Török,[2] and Fu-Jen Kao[1,*]

[1]*Institute of Biophotonics, National Yang-Ming University, 155, Li-Nong St. Taipei 11221, Taiwan*
[2]*Blackett Laboratory, Department of Physics, Imperial College London, Prince Consort Road, London SW7 2BZ, UK*
[*]*fjkao@ym.edu.tw*

Abstract: We developed a four-channel photon counting based Stokes-polarimeter for spatial characterization of polarization effects in second harmonic generation (SHG). We have implemented a calibration technique allowing quantitative measurement of polarization parameters, such as the degree of polarization (DOP), degree of linear polarization (DOLP), degree of circular polarization (DOCP), as well as anisotropy from the acquired Stokes parameters. The technique is used as contrast mechanism to characterize the polarization properties from two potassium dihydrogen phosphate (KDP) micro-crystals and collagen type-I in SHG microscopy.

OCIS codes: (180.4315) Nonlinear microscopy; (120.5410) Polarimetry; (320.0320) Ultrafast optics; (120.0120) Instrumentation, measurement, and metrology.

References and links

1. P. J. Campagnola and L. M. Loew, "Second-harmonic imaging microscopy for visualizing biomolecular arrays in cells, tissues and organisms," Nat. Biotechnol. **21**(11), 1356–1360 (2003).
2. A. D. Slepkov, A. Ridsdale, H. N. Wan, M. H. Wang, A. F. Pegoraro, D. J. Moffatt, J. P. Pezacki, F. J. Kao, and A. Stolow, "Forward-collected simultaneous fluorescence lifetime imaging and coherent anti-Stokes Raman scattering microscopy," J. Biomed. Opt. **16**(2), 021103 (2011).
3. E. Bélanger, S. Bégin, S. Laffray, Y. De Koninck, R. Vallée, and D. Côté, "Quantitative myelin imaging with coherent anti-Stokes Raman scattering microscopy: alleviating the excitation polarization dependence with circularly polarized laser beams," Opt. Express **17**(21), 18419–18432 (2009).
4. F. Lu, W. Zheng, and Z. Huang, "Heterodyne polarization coherent anti-Stokes Raman scattering microscopy," Appl. Phys. Lett. **92**(12), 123901 (2008).
5. W. R. Zipfel, R. M. Williams, R. Christie, A. Y. Nikitin, B. T. Hyman, and W. W. Webb, "Live tissue intrinsic emission microscopy using multiphoton-excited native fluorescence and second harmonic generation," Proc. Natl. Acad. Sci. U.S.A. **100**(12), 7075–7080 (2003).
6. D. Débarre, W. Supatto, A. M. Pena, A. Fabre, T. Tordjmann, L. Combettes, M. C. Schanne-Klein, and E. Beaurepaire, "Imaging lipid bodies in cells and tissues using third-harmonic generation microscopy," Nat. Methods **3**(1), 47–53 (2006).
7. R. W. Boyd, Nonlinear Optics(Academic press, San Diego, CA, 1992).
8. S. Psilodimitrakopoulos, S. I. C. O. Santos, I. Amat-Roldan, A. K. N. Thayil, D. Artigas, and P. Loza-Alvarez, "In vivo, pixel-resolution mapping of thick filaments' orientation in nonfibrilar muscle using polarization-sensitive second harmonic generation microscopy," J. Biomed. Opt. **14**(1), 014001 (2009).
9. R. Gauderon, P. B. Lukins, and C. J. R. Sheppard, "Three-dimensional second-harmonic generation imaging with femtosecond laser pulses," Opt. Lett. **23**(15), 1209–1211 (1998).
10. M. Strupler, A. M. Pena, M. Hernest, P. L. Tharaux, J. L. Martin, E. Beaurepaire, and M. C. Schanne-Klein, "Second harmonic imaging and scoring of collagen in fibrotic tissues," Opt. Express **15**(7), 4054–4065 (2007).
11. Y. Sun, W. L. Chen, S. J. Lin, S. H. Jee, Y. F. Chen, L. C. Lin, P. T. C. So, and C. Y. Dong, "Investigating mechanisms of collagen thermal denaturation by high resolution second-harmonic generation imaging," Biophys. J. **91**(7), 2620–2625 (2006).
12. V. Da Costa, R. Wei, R. Lim, C. H. Sun, J. J. Brown, and B. J. F. Wong, "Nondestructive imaging of live human keloid and facial tissue using multiphoton microscopy," Arch. Facial Plast. Surg. **10**(1), 38–43 (2008).
13. M. Han, G. Giese, and J. F. Bille, "Second harmonic generation imaging of collagen fibrils in cornea and sclera," Opt. Express **13**(15), 5791–5797 (2005).

14. P. Matteini, F. Ratto, F. Rossi, R. Cicchi, C. Stringari, D. Kapsokalyvas, F. S. Pavone, and R. Pini, "Photothermally-induced disordered patterns of corneal collagen revealed by SHG imaging," Opt. Express **17**(6), 4868–4878 (2009).
15. S. V. Plotnikov, A. C. Millard, P. J. Campagnola, and W. A. Mohler, "Characterization of the myosin-based source for second-harmonic generation from muscle sarcomeres," Biophys. J. **90**(2), 693–703 (2006).
16. P. J. Campagnola, "Second harmonic generation imaging microscopy: applications to diseases diagnostics," Anal. Chem. **83**(9), 3224–3231 (2011).
17. X. Chen, O. Nadiarynkh, S. Plotnikov, and P. J. Campagnola, "Second harmonic generation microscopy for quantitative analysis of collagen fibrillar structure," Nat. Protoc. **7**(4), 654–669 (2012).
18. E. Hecht, Optics, 4th ed. (Addison Wesley, 2002).
19. M. J. Walker, "Matrix calculus and the Stokes parameters of polarized radiation," Am. J. Phys. **22**(4), 170–174 (1954).
20. W. Bickel and W. Bailey, "Stokes Vectors, Mueller matrices and polarized scattered light," Am. J. Phys. **53**(5), 468–478 (1985).
21. M. R. Antonelli, A. Pierangelo, T. Novikova, P. Validire, A. Benali, B. Gayet, and A. De Martino, "Mueller matrix imaging of human colon tissue for cancer diagnostics: how Monte Carlo modeling can help in the interpretation of experimental data," Opt. Express **18**(10), 10200–10208 (2010).
22. N. Ghosh, M. F. G. Wood, and I. A. Vitkin, "Influence of the order of the constituent basis matrices on the Mueller matrix decomposition-derived polarization parameters in complex turbid media such as biological tissue," Opt. Commun. **283**(6), 1200–1208 (2010).
23. S. Y. Lu and R. A. Chipman, "Interpretation of Mueller matrices based on polar decomposition," J. Opt. Soc. Am. A **13**(5), 1106–1113 (1996).
24. E. Compain, S. Poirier, and B. Drevillon, "General and self-consistent method for the calibration of polarization modulators, polarimeters, and mueller-matrix ellipsometers," Appl. Opt. **38**(16), 3490–3502 (1999).
25. I. Berezhnyy and A. Dogariu, "Time-resolved Mueller matrix imaging polarimetry," Opt. Express **12**(19), 4635–4649 (2004).
26. L. M. S. Aas, P. G. Ellingsen, and M. Kildemo, "Near infra-red Mueller matrix imaging system and application to retardance imaging of strain," Thin Solid Films **519**(9), 2737–2741 (2011).
27. P. Schön, F. Munhoz, A. Gasecka, S. Brustlein, and S. Brasselet, "Polarization distortion effects in polarimetric two-photon microscopy," Opt. Express **16**(25), 20891–20901 (2008).
28. E. Y. S. Yew and C. R. J. Sheppard, "Effects of axial field components on second harmonic generation microscopy," Opt. Express **14**(3), 1167–1174 (2006).
29. P. Schön, M. Behrndt, D. Ait-Belkacem, H. Rigneault, and S. Brasselet, "Polarization and phase pulse shaping applied to structural contrast in nonlinear microscopy imaging," Phys. Rev. A **81**(1), 013809 (2010).
30. R. M. A. Azzam, "Arrangement of four photodetectors for measuring the state of polarization of light," Opt. Lett. **10**(7), 309–311 (1985).
31. S. Brasselet, D. Aït-Belkacem, A. Gasecka, F. Munhoz, S. Brustlein, and S. Brasselet, "Influence of birefringence on polarization resolved nonlinear microscopy and collagen SHG structural imaging," Opt. Express **18**(14), 14859–14870 (2010).
32. L. Fu and M. Gu, "Polarization anisotropy in fiber-optic second harmonic generation microscopy," Opt. Express **16**(7), 5000–5006 (2008).
33. C. W. Sun, C. C. Yang, and Y. W. Kiang, "Optical imaging based on time-resolved Stokes vectors in filamentous tissues," Appl. Opt. **42**(4), 750–754 (2003).
34. J. G. Webster, "Polarization measurement," in The Measurement, Instrumentation and Sensors Handbook, (CRC Press, 1998), Chap. 60.
35. M. Wolman and F. H. Kasten, "Polarized light microscopy in the study of the molecular structure of collagen and reticulin," Histochemistry **85**(1), 41–49 (1986).
36. M. R. Foreman, C. Macias Romero, and P. Török, "A priori information and optimisation in polarimetry," Opt. Express **16**(19), 15212–15227 (2008).
37. J. Qiu, Modern Optics Laboratory, National Yang-Ming University, 155 Li-Nong St, Taipei 112, Taiwan and N. Mazumder are preparing a manuscript to be called "Stokes vector formalism based nonlinear optical microscopy."
38. S. W. Chu, S. Y. Chen, G. W. Chern, T. H. Tsai, Y. C. Chen, B. L. Lin, and C. K. Sun, "Studies of $\chi^{(2)}/\chi^{(3)}$ tensors in submicron-scaled bio-tissues by polarization harmonics optical microscopy," Biophys. J. **86**(6), 3914–3922 (2004).
39. R. M. Williams, W. R. Zipfel, and W. W. Webb, "Interpreting second-harmonic generation images of collagen I fibrils," Biophys. J. **88**(2), 1377–1386 (2005).
40. E. W. Meijer, E. E. Havinga, and G. L. J. A. Rikken, "Second-harmonic generation in centrosymmetric crystals of chiral molecules," Phys. Rev. Lett. **65**(1), 37–39 (1990).
41. J. C. Mansfield, C. P. Winlove, J. Moger, and S. J. Matcher, "Collagen fiber arrangement in normal and diseased cartilage studied by polarization sensitive nonlinear microscopy," J. Biomed. Opt. **13**(4), 044020 (2008).
42. A. Periasamy, D. H. Burns, D. N. Holdren, G. H. Pollack, and K. Trombitás, "A-band shortening in single fibers of frog skeletal muscle," Biophys. J. **57**(4), 815–828 (1990).
43. W. Min, S. Lu, S. Chong, R. Roy, G. R. Holtom, and X. S. Xie, "Imaging chromophores with undetectable fluorescence by stimulated emission microscopy," Nature **461**(7267), 1105–1109 (2009).

1. Introduction

Optical imaging techniques based on nonlinear optical phenomena have been widely incorporated in microscopy using ultra-fast pulsed lasers. There have been many applications in cellular and tissue imaging because of the ability to spatially resolve subcellular details with high molecular contrast [1]. The development of nonlinear microscopy involving a wide range of contrast mechanisms, such as two-photon excitation fluorescence (TPEF) [2], second and third harmonic generation (SHG-THG) [1] and Coherent anti-Stokes Raman Scattering (CARS) has demonstrated immense capacity to the biological contrasts with high resolution, though usually with sub-millimeter depth penetration [2–4]. These imaging techniques have opened new routes towards optical diagnostics of complex cellular assemblies and tissue imaging [5,6].Second harmonic generation (SHG), a label free imaging technique, which arises from non-centrosymmetric structures [7] and the SH intensity depends on the relative orientation between the polarization of the incoming light and the second-order hyper polarizability of the sample [8]. Going beyond intensity measurements, SHG polarimetry can provide an interesting way to probe the absolute molecular structure orientation and disorder in organized organic media [1,6], impurities in crystal structures, characteristics of surfaces and optical interfaces [9]. Recently, SHG polarization anisotropy has been successfully applied to investigate the molecular orientation and the degree of organization in fibrotic collagen [10], human dermis [11], keloid [12], cornea [13,14], microtubules [8] as well as myosin of the skeletal muscle [15–17].

When light propagates through a sample to micrometer depths, the incoming light suffers a distortion in polarization induced by the sample. Spatially resolved polarization measurements permit detailed analysis of the changes in the magnitude and sign of the polarization parameters, and give information about the general symmetry properties of molecules. Polarization analysis can be carried out by Jones calculus, however this matrix method is applicable only for fully polarized light [18], whereas Stokes algebra is better for light in all states, whether incoherent, partially polarized or unpolarized [19,20]. A general beam of light can be characterized completely by four quantities known as the "Stokes parameters". Any optical device that changes the polarization of a light wave can be represented by 4 × 4 Mueller matrix.

Measurement of polarization properties from biological tissues has a number of biomedical applications, which benefit from the measurements of sample retardance, anisotropy via birefringence, diattenuation and depolarization of the scattering light [21,22].These polarization parameters can be fully determined using Lu-Chipman Mueller matrix decomposition techniques [23,24].To date, most studies have been made with linear optical technique [22,25,26], however SH light is sensitive to molecular structure and can provide detailed three-dimensionally resolved image contrast from biological samples.

Polarization microscopy imaging using an epi-geometry can lead to a undesired changes in the retrieved information, due to the degree of ellipticity of reflections from galvo-mirrors and dichroic mirrors [27]. In addition, the use of high numerical aperture objectives causes polarization distortions in excitation and detection arms [27]. These polarization distortions from various components in the optical path have been addressed and can be accounted for [28,29]. To perform quantitative polarimetry, we developed an imaging system which can measure the full Stokes parameters of the SH light using the transmission geometry. The light is analyzed byte Stokes-Mueller formalism [30], from which the degree of polarization and anisotropy through the birefringence of the sample can be found. Conventional SH polarization microscopy is used for examining the linear birefringence and polarization anisotropy of samples [31,32], but it is unable to measure the output polarization states of SH light. For comparison, our method provides a complementary technique to obtain the four Stokes parameters of the output signals from the samples when illuminated by different polarizations, which is similar to that of linear light scattering detection [33]. Determining the

polarization states in this way can reveal additional information regarding e.g. the circular birefringence properties of the SH light.

In this work, we have developed a four-channel photon counting based polarization microscope to determine the complete polarization states of SH light from the anisotropic samples, which are widely studied in molecular and biological sciences. A theoretical model is also carefully implemented to test the setup and to interpret the resultant images. This method is applied to analysis the representative photonic materials and fibrillar structures of bio-molecules, namely potassium dihydrogen phosphate (KDP), a standard nonlinear optical crystal and collagen type-I, respectively.

2. Materials and methods

2.1. Microscopy setup

A schematic diagram of the experimental arrangement for measuring the polarization properties of the signal in SHG microscope is shown in Fig. 1. A femtosecond Ti:Sapphire (Coherent Mira Optima 900-F) laser oscillator was used as the excitation light source. The source had a center wavelength of 800 nm and a full width at half maximum (FWHM) spectral width of 15 nm pulses with duration of ~100 fs, average power ~550 mW and repetition rate~76 MHz. The samples were mounted in upside-down on XYZ stage and scanned with a laser scanning unit (Olympus, FV300).The polarized beam of diameter 5 mm and average power of ~15mW before objective was focused onto the sample using an oil immersion objective lens (UPlanFLN 40X/N.A. 1.3 oil, Olympus Corp., Japan). The average powers of the laser beam on the sample surface were ~3mW and ~12mW for KDP crystals and collagen type-I, respectively. The measured signals are analyzed by means of a polarization state analyzer (PSA), specifically, a four-channel Stokes-polarimeter.

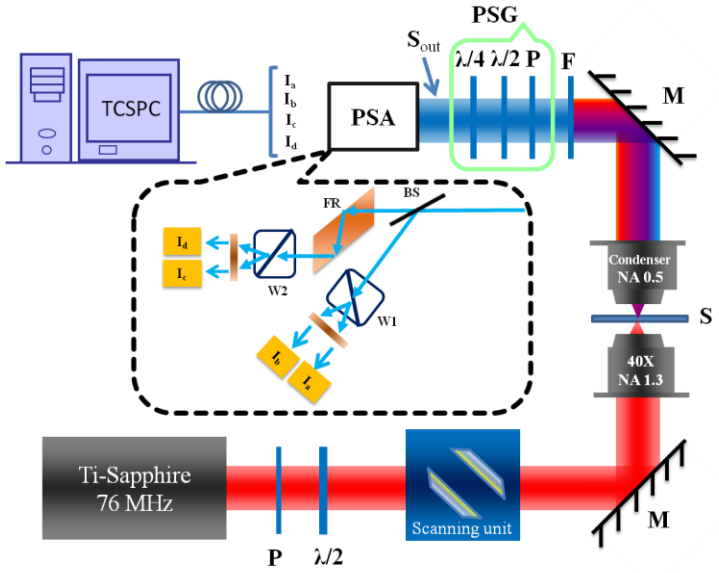

Fig. 1. Schematic diagram of polarization-resolved SHG microscope with four-channel Stokes -polarimeter module. The insert displays the polarization state analyzer (PSA);PSG: polarization state generator; P: Polarizer, λ/2: Half wave-plate, λ/4: Quarter wave-plate, M: Mirror, S: Sample, F: Filter, BS: Beam splitter, FR: Fresnel Rhomb,W1 and W2: Wollaston prisms, Ia, Ib, Ic, Id: photo-multiplier tubes (PMTs).

2.2. Working principle of four-channel Stokes-polarimeter

Figure 1 shows the four-channel Stokes-polarimeter imaging configuration. The SHG signals were collected in the forward direction by a long-working distance, 0.5 N.A. condenser. A band pass filter of 400 ± 40 nm (Edmund Optics Inc. Barrington, New Jersey) was inserted in the SHG emission path that is centrally peaked at 400 nm. An additional short pass filter (Brightline680 SP, Semrock) was used to discriminate the 800 nm excitation light. The resulting polarization state of SH signal is analyzed by a polarization state analyzer (PSA) is shown in Fig. 1. The PSA consists of a beam splitter (BS), Wollaston prisms (W1 and W2; WP 10, Thorlabs), Fresnel rhomb (FR; FR 600 QM, Thorlabs), and photon counting photo-multiplier tubes (PMTs; PMA 185 model, PicoQuant GmbH, Berlin, Germany). The SH signal is divided into two by a beam splitter, and then split further by two Wollaston prisms oriented at 45° with respect to the plane of incidence. Before separation by W2, the signals are passed through a Fresnel rhomb which works as a quarter wave plate to analyze the circular polarization. Stokes images 'Sout' from the SH signals are determined from the four intensity images acquired with 256 × 256 pixels spatial resolution, with 50 μm to 50 μm scanning area, using a pixel dwell time of 8μs by $S_{out} = (A_{4\times4})^{-1} \cdot I$,which are collected by PMTs through standard multimode fibers(FT1500EMT, 1.5 mm core diameter,0.39 N.A., Thorlabs). Here A4x4is the instrument matrix of the PSA. The signals are coordinated by four-channel detector router (PHR 800,PicoQuant GmbH, Berlin, Germany).Data collection and primary analysis is achieved by a commercial software package (SymPhoTime, PicoQuant GmbH, Berlin, Germany).

The initial steps of polarimetric experiments are to identify the principal axis of all the polarization components of the apparatus. After determining the principal axes, it is convenient to rotate the components to whatever angles specified. The basic scheme of our design is based on that of Azzam et al. [30], who introduced a four-detector based polarimeter that is capable of determining all four Stokes parameters of light. Our four-channel Stokes-polarimeter is a variation in that we detect SHG signals and reconstruct the 2D Stokes images using a laser scanning microscope in pixel by pixel analysis. A schematic drawing of the Stokes-polarimeter is shown in Fig. 1. The four-channel Stokes-polarization microscope consists of three distinct modules: a polarization state generator (PSG), the sample, and the polarization state analyzer (PSA). The PSG is combination of a linear polarizer (LPUV 100-MP, Thorlabs), a half wave-plate (AHWP05M-600, achromatic HWP, Thorlabs), and a quarter wave-plate (AQWP05M-600, achromatic QWP, Thorlabs) required to generate arbitrary polarization states. For comparison, the PSA consists of a beam splitter, Wollaston prisms, Fresnel rhomb, and photomultiplier tubes.

2.3. Stokes-parameters

Light of all polarization states can be characterized by four quantities known as the "Stokes-parameters" [34]. A Stokes vector, S describes a polarization state using four components, which are labeled as S0, S1, S2, and S3, where S0 is the total intensity, S1 is the intensity difference between linear polarization states at 0° and 90°, S2 is the intensity difference between linear polarization states at 45° and −45°, and S3 is the intensity difference between left-handed (LCP) and right-handed circular (RCP) polarization states, respectively. Thus, any change of polarization state of a beam would be represented by the 4-Stokes vector:

$$S = \begin{bmatrix} S_0 \\ S_1 \\ S_2 \\ S_3 \end{bmatrix} = \begin{bmatrix} I_0 + I_{90} \\ I_0 - I_{90} \\ I_{45} - I_{-45} \\ I_{\mathrm{RCP}} - I_{\mathrm{LCP}} \end{bmatrix} \quad (1)$$

where subscripts on I are the intensities at 0°, 90°, 45°, −45°, RCP and LCP states, respectively. The light input to the Stokes-polarimeter is represented by the Stokes vector Sout = [S0S1S2S3] t, where t stands for the transpose. The response of the Stokes-polarimeter to the incoming light is given by four intensities I = [IaIbIcId]t as shown in Fig. 1. The 4 × 1 intensity column vector 'I' (counts per msec) detected by time-correlates single photon counting (TCSPC) electronics, is given by the product of the4 × 4 instrument matrix A4x4 of the Stokes-polarimeter and the4 × 1 Stokes vector Sout of the SH signal:

$$I = A_{4\times4} \cdot S_{\text{out}} \tag{2}$$

Since I is the detected intensity vector, and A4x4 is a fixed matrix for a fixed configuration, Sout can be calculated as $S_{\text{out}} = \left(A_{4\times4}\right)^{-1} \cdot I$. The degree of polarization (DOP), the degree of linear polarization (DOLP), the degree of circular polarization (DOCP) and the anisotropy ratio of the SH light at each pixel of the scanning area are defined by the following equations:

$$\text{DOP} = \frac{\sqrt{S_1^{\,2} + S_2^{\,2} + S_3^{\,2}}}{S_0} \tag{3}$$

$$\text{DOLP} = \frac{\sqrt{S_1^{\,2} + S_2^{\,2}}}{S_0} \tag{4}$$

$$\text{DOCP} = \frac{|S_3|}{S_0} \tag{5}$$

$$r = \frac{I_{\text{par}} - I_{\text{perp}}}{I_{\text{par}} + 2I_{\text{perp}}} \tag{6}$$

For linear horizontal excitation, 'r' can be written as:

$$r = \frac{2S_1}{3S_0 - S_1} \tag{7}$$

DOP indicates the polarization property of the light. This value ranges from 0 to 1. If light is perfectly polarized, then DOP = 1. For an unpolarized light Stokes vectors are S0 = 1, S1 = S2 = S3 = 0, with DOP = 0. For partially polarized light, DOP is between 0 and 1, depending on the degree of polarization [34]. The DOLP indicates the crystalline alignment of molecules parallel to the linear polarization states; DOLP is between 0 and 1. The DOCP is a measure of how effectively the molecules flip the circularly scattered light within the focal volume; DPCP is between 0 and 1. The 'r' represents the anisotropy of the signals; 'r' is between –0.5 to 1.We have developed a series of specialized routines with MATLAB (MathWorks, R2009b) to reconstruct the two-dimensional intensity images as well as the corresponding Stokes vector and different polarization parameter images.

2.4. Sample preparation

The capability of the Stokes-polarimeter for measuring polarization properties is carried out by obtaining SHG signals from KDP micro-crystals and collagen type-I fibers. SHG imaging has been widely applied to collagen type-I fibers [10,11]. Collagen type-I forms cylindrical arrays of polypeptide coils comprising glycine-proline helices; it is strongly positively birefringent in respect to the length of the individual fibers [35].By varying the polarization states of the incident beam and detecting the change of polarization components after the samples, we reconstruct 2D Stokes SHG images of KDP micro-crystals (SIGMA, Germany)

and collagen type-I (Bovine Achilles Tendon, SIGMA, Germany). The KDP crystals and collagen type-I fibers were sandwiched between two cover glass slips. The samples were mounted upside-down in the microscope stage. From these reconstructed 2D Stokes vector images we can measure the DOP, DOLP, DOCP and the anisotropy ratio of the SH signal for every pixel in the image.

3. Results and discussion

3.1. Calibration

To accurately measure the Stokes vector of SH signals from the sample, the instrument matrix 'A4x4' for the polarimeter needs to be well known. The instrument matrix is determined with a set of known polarization states. These polarization states are generated after the sample position for calibration. SHG at 400 nm is created by focusing the 800 nm laser beam into KDP micro-crystals. The SH light is collimated by the condenser lens then passes through the PSG as described in the Materials and methods to generate the 0°, 90°, 45°and RCP states. The Stokes-polarimeter is calibrated using an eigen value calibration method [24,36], with these known polarization states. The performance of the Stokes-polarimeter is parameterized by the condition number of the instrument matrix 'A4x4', which is defined by $C = \|A_{4\times4}\| \cdot \left\|\left(A_{4\times4}\right)^{-1}\right\|$ where $\|\cdots\|$ denotes the L2-norm. In order to maintain high measurement accuracy, the condition number should be as low as possible [36].We have optimized our four-channel Stokes-polarimeter at 400 nm wavelength by minimizing the propagation of relative errors on the intensities after the multiplication with instrument matrix (A4x4)−1.

The instrument matrix 'A4x4' at 400 nm is given by-

$$A_{4\times4} = \begin{bmatrix} 292.88 & -209.49 & -216.62 & -0.75 \\ 213.26 & -60.71 & 166.99 & 19.41 \\ 267.48 & 84.15 & -78.93 & -209.49 \\ 250.91 & 72.30 & 32.95 & 247.98 \end{bmatrix} \quad (8)$$

The 16 numerical values in the matrix were determined by creating light of four known polarization states and counting photons on each of the four detectors for a fixed interval of time for each of these input states. We typically tuned the PSA to achieve a condition number of the instrument matrix of 3.0.The performance and accuracy of the four-channel Stokes-polarimeter are discussed in details in [37]. The PSG is removed once the instrument is calibrated.

3.2. SHG polarization-resolved imaging in KDP micro-crystals

Figure 2 show the Stokes vector SHG images of KDP micro-crystals from the microscope system combined with four-channel Stokes-polarimeter, when the laser with horizontal polarization is used. The Stokes parameter (S0) shows the SHG intensity image, and from this we are not able to distinguish the polarization properties of SHG signals. SHG polarization-resolved experiments are traditionally carried out by rotating an analyzer before the detector [31] and the SHG anisotropy patterns are obtained by analyzing the selected number of pixels of the images [32,38,39]. Here we are using256 × 256 pixel analysis of 2D reconstructed Stokes images without relying on any sample alignment or analyzer rotation. Figures 2(a) and 2(b) show the 2D Stokes images of output polarizations states and different polarization properties of SHG signals from KDP micro-crystals, for an incident horizontally polarized beam. In such geometry, the excitation field propagates through the whole thickness of the sample. The two KDP micro-crystals show significant differences in polarization characteristics, which is due to the birefringent behavior of the micro-crystals [32].

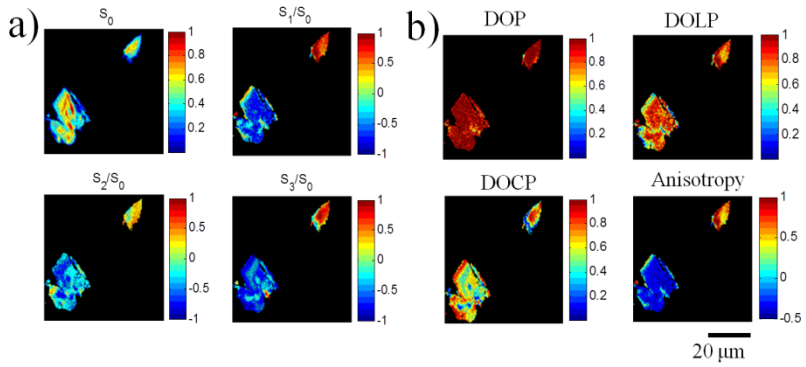

Fig. 2. Experimental polarization-resolved SHG response from KDP micro-crystals,(a) shows the reconstructed 2D Stokes vector images; (b) represents the DOP, DOLP, DOCP and polarization anisotropy images of SHG light from the KDP micro-crystals, when the input polarization is horizontal polarized. The color scale shows the values of each parameter.

As shown in Fig. 2(b), the DOP from two KDP micro-crystals is approximately 1, indicating that most of the excited SH signal is polarized. The DOLP and the DOCP images demonstrate that there exist both linear and circular polarization states in the SHG light from the KDP micro-crystals. Linear and circular polarization is generated from the KDP micro-crystals due to the birefringence property of the crystals. For the smaller KDP micro-crystal in the upper right hand corner (Fig. 2(b)), there are larger components of linear horizontal and right circular polarization. For comparison, there are larger components of linear vertical and left circular polarization for the KDP micro-crystal in the lower left hand corner. Since birefringence gives rise to a variation of relative phase between field components with propagation depth, hence changing an incoming linear light to an oscillatory function between circular and linear. A variation of polarization is seen dependent on propagation length in the crystal. In general the field is elliptically polarized i.e. one circular polarization will dominate the other [40]. The SH anisotropy image also shows the orientation differences of the KDP micro-crystals. The smaller crystal gives rise to greater anisotropy than the other.

3.3. SHG polarization resolved imaging in collagen

SHG imaging has been widely applied to collagen type-I fibers [10,11]. The structural information from collagen type-I fibers can be understood more precisely by polarization-resolved SHG imaging [1,2,17]. Previous studies reported that SHG sources lie within the amide bonds of polypeptide chains in collagen type-I [15,17]. Figures 3(a) and 3(b) displays the linear polarization effects the affect of polarization properties of SHG signals of thick type-I collagen. The normalized Stokes vector images (Fig. 3(a)) of the SHG signals are obtained from collagen type-1 fibers, with an incident beam is horizontal polarized.

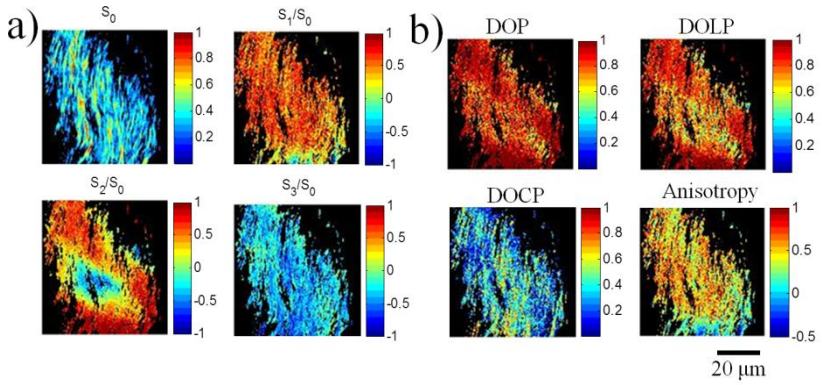

Fig. 3. Experimental polarization-resolved SHG response from collagen type-I, (a) shows the reconstructed 2D Stokes vector images; (b) represents the DOP, DOLP, DOCP and polarization anisotropy images of SHG light from the collagen type-I, when the input polarization is horizontal polarized. The color scale shows the values of each parameter.

The Stokes images (Fig. 3(a)) shows that the relative phase shift via the light propagation through the whole collagen fiber, again changes an incoming linear polarization state to an oscillatory function between linear (S1, S2) and circular (S3) polarization state dependent on propagation depth. Due to the structural property of collagen, it is possible to produce partially polarized states of polarization [35]. This is clear evidence of a progressive rotation of the collagen fiber or the orientation of the optical axis of molecules. The DOLP indicates the crystalline alignment of fiber and molecules parallel to the linear polarization states. The optical activity of collagen can also be observed with SH light. The DOCP is a measure of how effectively the collagen flips the helicity of the scattered light within the focal volume. The chirality in collagen affects the SH polarization, resulting in a polarization shift away from both fundamental and SH signal produced by the sample. This shift is clearly visible in the DOCP image and the SH signal is a mixture of both right and left circularly polarized light. The effect of birefringence on the SHG polarimetric data is explored via anisotropy measurement, which confirms the strong deformation for different areas of collagen [41]. Observation of the polarization parameters reveals that collagen fibrils are highly anisotropic, coinciding with the known pitches of distinct helices within the coil structure of collagen. Polarization-resolved SHG Stokes vector imaging can hence be used to visualize the structural distribution in highly ordered biological samples through inspection of different polarization properties. This technique may be very powerful tool in investigating the structural dynamics in skeletal muscle fiber under the physiological conditions [42] for example.

4. Conclusion

In conclusion, we have constructed a four-channel Stokes vector based imaging polarimeter for second harmonic generation microscopy. By analyzing the Stokes images, obtained from the SHG signal, we are able to quantify the polarization state of arbitrarily polarized light, the DOP, the DOLP, the DOCP and polarization anisotropy of SH signal to visualize the birefringence and crystal orientation from KDP and collagen type-I. This newly developed instrument which measures different polarization properties and information contained in SH light has valuable applications in biology. The method still has room for improvement, both to reduce experimental errors as well as improving the interpretation of results. Current work is under progress to further increase the amount of information that can be derived from polarization parameters. The polarization study or characterization can be easily extended to polarization maintaining optical processes and signals, which include harmonics generation (second and third), CARS, stimulated emission [43] microscopy. Additionally, time-resolved

and polarization-resolved investigation on fluorescence may yield unprecedented information on the dynamics of molecules.

Acknowledgments

We appreciate greatly Dr. Andy Ridsdale and Prof. Albert Stolow from National Research Council, Canada for fruitful discussions on implementing Stokes vector based methods. The insightful discussion with Prof. Tsu-Wei Nee was crucial in interpreting the results. The authors would also like to thank the National Science Council, Taiwan (NSC99-2627-M-010-002, NSC98-2627-M-010-006, NSC97-2112-M-010-002-MY3, and NSC98-2112-M-010-001-MY3), as well as the Ministry of Education, Taiwan under the "Aim for Top University" project for the generous support of the reported work.